Accepted Manuscript

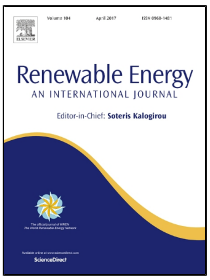

Experimental and Numerical Investigation of the Hydrodynamic Performance of an Oscillating Water Column Wave Energy Converter

K. Rezanejad, C. Guedes Soares, I. López, R. Carballo

PII:	S0960-1481(17)30003-4
DOI:	10.1016/j.renene.2017.01.003
Reference:	RENE 8441
To appear in:	*Renewable Energy*
Received Date:	23 May 2016
Revised Date:	30 December 2016
Accepted Date:	02 January 2017

Please cite this article as: K. Rezanejad, C. Guedes Soares, I. López, R. Carballo, Experimental and Numerical Investigation of the Hydrodynamic Performance of an Oscillating Water Column Wave Energy Converter, *Renewable Energy* (2017), doi: 10.1016/j.renene.2017.01.003

Experimental and Numerical Investigation of the Hydrodynamic Performance of an Oscillating Water Column Wave Energy Converter

K. Rezanejad [1], C. Guedes Soares [2]* , I. López [3] & R. Carballo [4]

[1,2] Centre for Marine Technology and Ocean Engineering (CENTEC), Instituto Superior Técnico, Universidade de Lisboa, Av. Rovisco Pais, 1049-001 Lisboa, Portugal

[3,4] Hydraulic Engineering Area, Universidade de Santiago de Compostela, Campus Universitario s/n, 27002, Lugo, Spain

* Corresponding author e-mail: c.guedes.soares@centec.tecnico.ulisboa.pt

Highlights

The performance of an oscillating water column converter is investigated numerically and experimentally

The boundary integral equation method is implemented to solve the appropriate 2D boundary value problem

A comprehensive experimental campaign is carried out in both regular and irregular waves.

the efficiency is very sensitive to the variations in the turbine damping although the absolute maximum efficiency is less sensitive

influence of the wave height has less important than the other two parameters (turbine damping and incoming wave period)

Experimental and Numerical Investigation of the Hydrodynamic Performance of an Oscillating Water Column Wave Energy Converter

K. Rezanejad [1], C. Guedes Soares [2]* , I. López [3] & R. Carballo [4]

[1,2] Centre for Marine Technology and Ocean Engineering (CENTEC), Instituto Superior Técnico, Universidade de Lisboa, Av. Rovisco Pais, 1049-001 Lisboa, Portugal

[3,4] Hydraulic Engineering Area, Universidade de Santiago de Compostela, Campus Universitario s/n, 27002, Lugo, Spain

* Corresponding author e-mail: c.guedes.soares@centec.tecnico.ulisboa.pt

Abstract

The performance of an oscillating water column wave energy converter is investigated based on both numerical and experimental approaches. The viscosity effects are neglected in the numerical approach and the boundary integral equation method (BIEM) is implemented to solve the appropriate 2D boundary value problem (BVP). The influence of turbine damping and wave period is evaluated in the numerical model in both regular and random waves. A comprehensive experimental campaign is carried out in both regular and irregular waves to validate the numerical results as well as to investigate the influence of wave height, period and turbine damping on the efficiency of the converter. High and low turbine damping conditions are imposed to the experimental model. It is found that both the numerical and experimental results have a satisfactory agreement for the small wave amplitudes. It is detected that the efficiency of the device is very sensitive to the variations in the turbine damping although the absolute maximum efficiency is less sensitive to the slight alterations applied to the turbine damping. It is observed in the experimental study that the influence of the wave height has less importance than the other two parameters (turbine damping and incoming wave period) although the effect of the wave height becomes prominent in high wave amplitudes and causes the efficiency of the device to become less sensitive to variations in wave period and to tend to have an uniform value in wide wave period ranges.

Keywords: Oscillating water column; hydrodynamic performance of OWC; turbine damping; boundary integral equation method; primary efficiency.

1. Introduction

Ocean wave energy is an indigenous resource in many regions/countries worldwide and is among the renewables with the greatest potential (Bahaj, 2011 and Cruz, 2008), but is still almost entirely untapped. The ever-growing need for sustainable, non-polluting electricity led to the development of a wide variety of technologies to harvest wave energy. This situation is not expected to decrease as new concepts tend to replace those that are being abandoned. However, only a few of the most promising concepts have proceeded to a demonstration testing phase at a pre-commercial scale, after a comprehensive physical and numerical modelling development plan, to minimize investment risks.

Amongst various devised wave energy converters (WEC), Oscillating Water Column (OWC) devices are one of the concepts successfully deployed around the world (Clement et al. 2002) which are expected to be one of the most popular WECs for viable wave energy harvesting. The OWC devices are considered to be advantageous over the many other existing devices: no moving parts are located in the water, the use of an air turbine eliminates the need for gearboxes, there is no need to implement underwater cables in fixed onshore types, their maintenance procedure is easy, there is an efficient usage of the sea space and they are environment friendly. A detailed general review of the existing concepts and designs of wave energy converters is available in Guedes Soares et al. (2012), Falcão (2010) and Falnes (2007).

Investigations regarding wave power extraction from water waves have started since the 1970s and were concentrated on rigid body models as described by Evans (1976), Evans (1981) and Mei (1976). Then, the uniform surface pressure model was implemented to analyze the performance of OWC devices in which the governing equations are expressed in terms of pressure on the OWC free surface and flow rate displacement by the OWC surface motion (Evans, 1982). Falnes and McIver (1985) further extended that work by designing a wave energy absorption system consisting of a number of oscillating bodies and internal pressure distributions.

Several attempts have been made in recent years to explore the performance characteristics of the various types of OWC devices. In this regard, Gervelas et al. (2011) presented numerical and experimental predictions on a model scale OWC using the one dimensional time domain model for regular and irregular waves. Ikoma et al. (2011) proposed an OWC device with an

artificial harbour surrounded by projecting walls to improve the efficiency of the wave power absorption. They performed experiments in support of their results and, thus, provided an estimate of the absorbed power by several types of OWC devices for the Japanese coast all over the year. Crema et al. (2015) performed experimental investigations on OWC WECs which are integrated into a very large floating structure. They assessed the influence of the size of the OWC chamber, the lip drought and the turbine damping on the hydraulic efficiency of the device in the both regular and random waves. López et al. (2014 a,b) conducted numerical and comprehensive experimental investigations to explore turbine damping effects as well as the influence of tidal conditions and wave characteristics on the performance of an OWC device. López and Iglesias (2014) developed a virtual laboratory that allowed the determination of the pneumatic efficiency of a given OWC working under specific conditions of incident waves (wave height and period), tidal level and turbine damping. Falcão and Henriques (2014) introduced a comprehensive review and investigation on the rules for geometric, hydrodynamic, thermodynamic and aerodynamic similarity in model testing of OWC devices.

As the nonlinear characteristics of the power take-off (PTO) system might have prominent influences on the WEC power absorption capacity and cannot be applied in the linear frequency domain analysis, Falcão et al. (2012) and Sheng et al. (2014 a,b) introduced a nonlinear time domain approach and applied corresponding nonlinearities in the dynamic motion equation of the oscillatory part of the WEC device.

Ning et al. (2015) investigated the hydrodynamic performance of an OWC wave energy device using a fully nonlinear HOBEM (higher-order boundary element method). Ning et al. (2016) performed an experimental campaign to analyze the influence of the bottom slope and geometric parameters on the performance of the OWC device. They found that the opening ratio (the ratio of cross-sectional area of the air-slot to cross-sectional area of the air chamber) had a significant influence on the performance of the OWC device. They reported that the bottom slope had little influence on the resonant frequency and that the optimal hydrodynamic efficiency increased with the bottom slope. Anvesh et al. (2016) investigated the influence of bottom sloping configuration located in front of the OWC on the performance of the device. They found that as the slope of the bottom configuration increases, the waves are reflected back which leads to decrease the capturing of wave energy from the PTO device.

Rezanejad et al. (2015 & 2016) studied the performance of two-dimensional nearshore dual chamber OWC devices based on linear potential theory in flat and stepped sea bottom condition. They proved that significant improvements in the primary efficiency of the device can be achieved by implementing dual chambers in an OWC converter and the device performance could be further improved by adding an appropriate step in the sea bottom.

This paper follows up on these last two works and aims to investigate the performance of an OWC device using both numerical and experimental approaches. The numerical model is developed based on linear wave theory in two dimensions as the experiments are also set up principally based on two dimensional configurations. The standard numerical technique using the two dimensional boundary integral equation method (BIEM) is used to obtain the solution for the associated boundary value problem (BVP). The implemented linear numerical approach establishes a straight forward solution to obtain a general prospective behaviour of the device in the both regular and random waves. However, several non-linear phenomena can occur (e.g. nonlinear hydrodynamic interactions, occurring vortices, influence of the nonlinear power take-off systems and nonlinear air compressibility effects) in the process of energy production which is linearized or neglected in the linear analysis. Hence, in order to provide the detailed perception of the device performance in reality the comprehensive experimental tests are carried out considering both regular and random waves. The validity of the numerical results is assessed by comparing the relevant results with the results achieved from experimental data for both regular and irregular waves. The work emphasizes the exploration of the influence of the wave characteristics (wave height and wave period) as well as turbine damping on the efficiency of the OWC wave energy converter.

2. Numerical modelling

2.1. Mathematical formulation

The mathematical model is based on the two-dimensional Cartesian coordinate system (x,z) with $x-$ axis being the horizontal axis and $z-$ axis being vertically upward positive. The origin of the coordinate system is placed at the point of intersection of the vertical rigid wall and the undisturbed free surface and hence it is situated at $x = 0$. The schematic diagram for the numerical model of OWC together with its geometrical parameters is shown in Figure 1. As shown in this figure, the sea bottom has a step located immediately under the OWC

opening. It is assumed that the water depth is equal to h_2 above the step and to h_1 outside of it and remains constant throughout the sea bed.

Under the linear water wave theory, the fluid is assumed to be inviscid, incompressible and the motion is irrotational and harmonic in time with angular frequency ω. Therefore, there is a velocity potential $\phi(x,z,t) = \mathrm{Re}\{\varphi(x,z)e^{-i\omega t}\}$, with the spatial velocity potential $\varphi(x,z)$ satisfying the following boundary value problem (BVP):

$$\nabla^2\varphi = 0, \text{ in the fluid region, } \nabla^2 \equiv \frac{\partial^2}{\partial x^2} + \frac{\partial^2}{\partial z^2} \quad (1)$$

$$\frac{\partial\varphi}{\partial z} = 0, \text{ on the sea bottom} \quad (2)$$

$$\frac{\partial\varphi}{\partial n} = 0, \text{ on the step, rigid walls and barrier of the OWC chamber} \quad (3)$$

$$\frac{\partial\varphi}{\partial z} - K\varphi = 0, \text{ on the water free surface outside of the OWC chamber} \quad (4)$$

$$\frac{\partial\varphi}{\partial z} - K\varphi = \frac{i\omega}{\rho g}p, \text{ on the water free surface inside of the OWC chamber} \quad (5)$$

where $K = \omega^2/g$ and p is the complex time independent imposed pressure distribution of the form $P(t) = \mathrm{Re}\{pe^{-i\omega t}\}$ over the internal free surface, $\vec{n}$ is the normal unit vector, ρ is the sea water density, and g is the gravitational acceleration.

Following the method of Evans & Porter (1995), the total potential $\varphi(x,z)$ is decomposed into two parts as follows:

$$\varphi = \varphi^S + \frac{i\omega p}{\rho g}\varphi^R \quad (6)$$

where φ^S is denoted as the scattered potential, which is associated with the scattering of a plane incident wave from $x = +\infty$ in the absence of an imposed pressure on the internal free surface and φ^R is the radiated potential, which is the solution of the radiation problem due to the pressure imposed on the internal free surface. The scattered potential φ^S satisfies Eqns. (1) – (5) with $p = 0$, while φ^R satisfies Eqns. (1) – (5) with Eqn. (5) replaced by:

$$\frac{\partial\varphi^R}{\partial z} - K\varphi^R = 1 \quad (7)$$

In order to find the scattered potential φ^S, according to the diffraction theory, it is assumed that the scattered potential is the decomposition of two parts: incident potential φ^I and diffracted potential φ^D.

The incident wave potential does not feel the existing bodies and hence, it can be obtained analytically using simple linear water wave theory:

$$\varphi^I = A\frac{i\omega}{k}\frac{\cosh k(h_1+z)}{\sinh kh_1}e^{-ikx} \tag{8}$$

where A is the amplitude of the wave and k represents the wave number and is the real root of the wave dispersion relation:

$$\omega^2 = gk\tanh kh_1 \tag{9}$$

Therefore, the rigid wall at $x = 0$ as well as the barrier and the step boundary condition for the diffracted potential φ^D takes the new form of the following formula in order to take into account the effects of the body existence on the incoming waves:

$$\frac{\partial\varphi_D}{\partial n} = -\frac{\partial\varphi_I}{\partial n}\text{, on the wall, step and barrier of the OWC chamber} \tag{10}$$

The rest of boundary conditions remain unchanged as before.

In addition, the Sommerfeld condition is used as the far field boundary condition in diffraction and radiation problems as follows:

$$\frac{\partial\varphi^{D,R}}{\partial x} - ik\varphi^{D,R} = 0 \quad \text{as} \quad x \to +\infty \tag{11}$$

The time harmonic induced volume flux $Q(t) = \mathrm{Re}\{qe^{-i\omega t}\}$ across the internal free surface following Evans & Porter (1995) is given by:

$$q = L\int_S \frac{\partial\varphi}{\partial z}dx = q^S + \frac{i\omega p}{\rho g}q^R \tag{12}$$

where L is the width of the chamber perpendicular to the incident wave direction, and q^S and q^R are the volume fluxes across the internal free surface S in the scattering and radiation problems, respectively.

The volume flux q^R for the radiation problem is separated into real and imaginary parts as in Evans & Porter (1995):

$$\frac{i\omega p}{\rho g}q^R = -(\hat{B} - i\omega\hat{A})p \tag{13}$$

where $\hat{A}$ and $\hat{B}$ are obtained as:

$$\hat{A} = \frac{1}{\rho g}\mathrm{Re}\{q^R\} \tag{14a}$$

$$\hat{B} = \frac{\omega}{\rho g}\mathrm{Im}\{q^R\} \tag{14b}$$

On the other hand, following Evans (1982), it is assumed that the total air volume flux through the turbine is linearly proportional to the pressure drop across the internal free surface. Therefore, by considering Eqns. (12-13) and taking into account linearized air compressibility inside of the chamber, the following relationship can be achieved between pressure and scattered volume flux after rearranging as:

$$p = (\lambda + \hat{B} - i\omega\hat{A} - \frac{i\omega V_0}{\gamma p_a})^{-1} q^S \tag{15}$$

where V_0 is the air volume above internal free surface and inside of the chamber, γ is the specific heat ratio of air which equals to 1.4, p_a is the atmospheric air pressure and λ has real positive value and is associated with damping induced by the linear turbine to the air flow as follows:

$$q = \lambda p \tag{16}$$

The mean rate of work $W_{Reg.}$ done by the pressure force over one wave period of a regular wave is given by (Evans, 1982):

$$W_{Reg.} = \frac{1}{2}\lambda|p|^2 \tag{17}$$

The available power over one wave period of a monochromatic wave is given by:

$$W_w = Ec_g \tag{18}$$

where E is the total energy per wave period and c_g is the group velocity and is given by (Dean & Dalrymple, 2001):

$$E = \frac{1}{2}\rho g L A^2 \tag{19}$$

$$c_g = \frac{1\omega}{2k}\left(1 + \frac{2kh_1}{\sinh 2kh_1}\right) \tag{20}$$

Thus, the primary efficiency $\eta_{Reg.}$ of the OWC device in regular waves is given by:

$$\eta_{Reg.} = \frac{W_{Reg.}}{W_w} \tag{21}$$

It is proved in the previous investigations that the solutions for the radiated and scattering problems are not independent from each other and hence the relation between them can be expressed as follows (Falnes, 2002):

$$\left|q^S\right|^2 = 8\hat{B}W_w \tag{22}$$

By substituting Eqns. (17) and (18) into Eqn. (21) and taking Eqn. (22) into account, the following simplified form for the efficiency expression of the OWC device in regular waves can be obtained:

$$\eta_{Reg.} = \frac{4\lambda\hat{B}}{(\lambda+\hat{B})^2 + \omega^2\left(\hat{A} + \frac{V_0}{\gamma p_a}\right)^2} \tag{23}$$

which is independent of the incident wave power and only depends on radiation solution.

It is noteworthy to highlight that in order to estimate the maximum primary efficiency $\eta_{Reg.,max}$ in each wave period of the regular wave, it is enough to substitute the optimum value of λ into Eqn. (23). The optimum value of λ can be evaluated as follows by applying zero value to the derivative of Eqn. (23) with respect to λ:

$$\lambda_{opt} = \sqrt{\hat{B}^2 + \omega^2(\hat{A} + \frac{V_0}{\gamma p_a})^2} \tag{24}$$

Hence, substituting Eqn. (24) into Eqn. (23) leads to the expression for the maximum efficiency of OWC device in regular waves as follows:

$$\eta_{Reg.,max} = \frac{2\hat{B}}{\lambda_{opt} + \hat{B}} \tag{25}$$

On the other hand, the method of Falcão & Rodrigues (2002) is implemented to analyze the performance of the OWC device in random waves using the solutions of the radiation and wave scattering problems in regular waves. In this regard, it is assumed that the local wave climate may be represented by a set of sea states, each being a stationary stochastic ergodic process and therefore the surface elevation being a Gaussian random variable for each sea

state. In this situation, the variance of the air pressure fluctuations σ_p^2 can be estimated as follows (Falcão & Rodrigues, 2002):

$$\sigma_p^2 = \int_0^\infty S(\omega)\left|\frac{p(\omega)}{A}\right|^2 d\omega \tag{26}$$

where $p(\omega)$ can be obtained from Eqn. (15) and $S(\omega)$ is the one-sided wave elevation spectrum.

Due to linear proportionality between pressure drop across the air turbine and total volume flux through it, the instantaneous power absorbed from sea waves $W_{absorbed}$ can be obtained as:

$$W_{absorbed} = \frac{\dot{m}P}{\rho_a} = \lambda P^2 \tag{27}$$

where $\dot{m}$ is the air mass flow across the turbine, P is the instantaneous relative air pressure amongst outside and inside the chamber, and ρ_a is the air density.

It should be noted that since it was assumed that the system is linear and the free surface elevation can be considered as a Gaussian random parameter, both Q^S and P are also Gaussian processes. Hence, according to Eqn. (27), the average power absorbed from random waves $W_{Ran.}$ in a specific sea state can be estimated as follows (Falcão & Rodrigues, 2002):

$$W_{Ran.} = E(W_{absorbed}) = \int_{-\infty}^{+\infty} W_{absorbed} f(P) dP \tag{28}$$

where $E(W_{absorbed})$ is the expectation value of absorbed power and $f(P)$ is the probability density function of instantaneous pressure which follows the Gaussian distribution:

$$f(P) = \frac{1}{\sqrt{2\pi}\sigma_p}\exp\left(-\frac{P^2}{2\sigma_p^2}\right) \tag{29}$$

By substituting Eqns. (27) and (29) into Eqn. (28) and solving the associated integral analytically, the mathematical expression of average absorbed power $W_{Ran.}$ can be stated in simpler form as (Falcão & Rodrigues, 2002):

$$W_{Ran.} = \lambda\sigma_p^2 \tag{30}$$

Hence, it is evident from Eqn. (30) that the average power absorbed from random sea waves is solely dependent on the turbine characteristics and the variance of air pressure inside the chamber and can be calculated from the results of the frequency domain solution for regular waves.

On the other hand, the average primary efficiency of the OWC device in random sea waves $\eta_{Ran.}$ for specific sea state can be evaluated as follows:

$$\eta_{Ran.} = \frac{W_{Ran.}}{\overline{W}_w} = \frac{\lambda \int_0^\infty S(\omega) \left|\frac{p(\omega)}{A}\right|^2 d\omega}{\overline{W}_w} \tag{31}$$

where $\overline{W}_w$ is the average incident wave energy flux for the random wave and can be calculated from the spectral density by:

$$\overline{W}_w = L\rho g \int_0^+{}^\infty S(\omega) c_g(\omega) d\omega \tag{32}$$

where $c_g(\omega)$ is the group velocity and can be calculated from Eqn. (20).

2.2. Method of solution

In this subsection, the numerical method applied for solving the associated BVP in the case of the OWC in the frequency domain is briefly described. The results of the frequency domain solution will be implemented in Eqns. (23), (25) and (31) for each frequency in order to analyze the performance of the OWC device.

The well-known BIEM is used to solve the radiation and diffraction problems separately. For solving the governing equation with appropriate boundary conditions using numerical approach, the distribution of all variables along the linear elements is assumed to be linear. Discretizing the Laplace equation based on the boundary element method, the fundamental integral equation for boundary points is obtained as (Paris et al. 1997):

$$c(X)\phi(X) + \int_{\partial D} \phi(Y) \frac{\partial \psi}{\partial n}(X,Y) ds(Y) = \int_{\partial D} \psi(X,Y) \frac{\partial \phi}{\partial n}(Y) ds(Y) \tag{33}$$

where ϕ is the unknown flow potential, $\partial\phi/\partial n$ is the derivative of the potential relative to normal unit vector on the boundary, ψ is the fundamental solution of Laplace equation, and ∂D is the boundary of consideration. Eqn. (33) relates the value of the flow potential at a fixed

point X to each and every arbitrary point Y on the entire boundary. The value of the parameter c which is called the free term depends only on the shape of the boundary and is equal to:

$$c(X) = \frac{\alpha(X)}{2\pi} \tag{34}$$

where $\alpha(X)$ is the angle between the two tangents of the boundary domain in the left and right hand sides of the point X.

The multi region concept is used to discretise the linear fundamental integral Eqn. (33), which diminishes the numerical errors arising from the small thickness of the front wall of the OWC device (see Rezanejad et al., 2013 & 2015 for details).

3. Experimental investigation

3.1. Physical model

The model for the shore line fixed OWC was built with the scale factor of 1:25 ($\varepsilon = 1/25$) to carry out the experimental campaign. The sketch of the model with its main dimensions as well as the tested physical one in the wave flume is illustrated in Figure 2. A Guarda region located in North West of Spain would be one of the appropriate locations to install prototype of the OWC examined in the present study, as reported by López et al., (2013) for the OWC with similar dimensions but with the different immersion depth of the lip. As the model was designed in such a way that occupied the whole width of the wave flume, the results achieved from the experimental campaign would be recognized as a 2D case and hence could be compared with the results gathered from the numerical solutions.

The following three main non-dimensional values have a dominant influence on the primary performance of OWC devices: Froude number (Fr), Reynolds number (Re) and dimensionless pressure. The Froude and Reynolds similarities cannot be satisfied simultaneously. In the model testing of floating objects, the effects due to variations in Froude number are almost always much more important than those associated with changes in Reynolds number (Falcão and Henriques, 2014). This is mainly due to the reason that a relative large Reynolds number in a scale model can be easily achieved in most practical cases and thus the viscous terms in the fluid momentum equation will become minor (see Sheng et al., 2014c for further details). Although the OWC studied here is not a floating OWC, the statement that changes in Froude number imply larger changes in the model similarity than

those related to changes in the Reynolds number, still remain a valid. Hence, Froude number was kept on the basis of the lessons learnt in previous studies and Reynolds number was ignored as a modelling rule. It should be noted that it is required to consider large quantities of air volume inside the OWC chamber if the dimensionless pressure is intended to be applied as a criterion to perform the experiments simultaneously with considering Froude similarity rule, but it is normally applicable for large model testing conditions and hence the simulation of the air compressibility effects was ignored in the experimental setup used for this study. Following the Froude similarity rule, the scale ratios for the most important parameters implemented in this paper are shown in Table 1.

As illustrated in Figure 2, the model was built from Plexiglas material due to its appropriate mechanical strength, simplicity in construction procedure and transparency which allowed the observation of the motions of the inside water free surface. In general, scaling ratios in wave energy converter model tests do not exceed 1:10 and hence leads to power ratio of about 1:3200 (see Table 1). In the case of an OWC wave energy converter, this scale is too small for the turbine to be adequately simulated by a mini-turbine. Hence, the usual procedure is to simulate the power take-off unit as an orifice or as a layer of porous material to apply the equivalent influence of the impulse or Wells turbine, respectively (Falcão and Henriques, 2014). The reason being that pressure drop across the orifice or the porous medium element varies quadraticaly or linearly with the flow rate, as it does across an impulse or Wells turbine, respectively (López et al. 2014b). The early developments of OWC technology were focused on Wells turbines; over the last years, however, research has been mainly directed toward impulse turbines (López et al. 2014b). Hence, the impulse turbine is selected here in this study as the power take-off unit acting on the OWC system. In this paper, the rectangular slot (instead of a circular orifice) was implemented in the top of the model to provide a more realistic 2D condition in the experiments. In this regard, two different slot widths ($e = 1$ and 2.5 mm) were applied to the model to impose high and low turbine damping conditions, respectively. The ratio of the cross sectional area of the slot to the water free surface area (OWC area) inside the chamber is consequently equal to 0.78% and 2% for the high and low damping conditions ($e = 1$ and 2.5 mm), respectively. In principle, the 1 mm slot width was chosen in the experimental setup based on the past investigations which reported the best performance of the OWC devices are mainly achieved when the slot area is around 1% of the cross sectional area of the OWC (e.g. Ashlin et al., 2016 illustrated that the best energy absorption is obtained when the slot area is about 0.68% of the OWC area). Furthermore, the

low damping condition ($e = 2.5\ mm$) is also investigated in the experimental part of this research study to explore the performance of the OWC device in various wave characteristics when the appropriate desired damping condition could not be imposed to the system.

3.2. Experimental setup and test design

The experimental tests were carried out in the wave flume of the University of Santiago de Compostela which is 20 m long, 0.65 m wide and 0.95 high. The flume has a piston-type wave generator with Active Wave Absorption Control System (AWACS) which has the capability to produce both regular and irregular waves. The sketch of the wave flume as well as the location of the corresponding wave gauge sensors and the OWC model is shown in Figure 3. As can be seen, the OWC model was located at 10.75 *m* distance from the mid-position of the wave paddle and occupied the whole width of the wave flume. Hence, the generated waves were not impressed by the wave dissipation ramp as some part of their energy were absorbed by the OWC model and the rest were reflected back to the wave generator upon interfacing with the model. As the wave generator system was equipped with the AWACS system, the reflected waves were absorbed automatically by the wave generator which eventually caused the incident wave pattern to remain undisturbed.

In order to detect water free surface elevation outside of the OWC model, eight resistive wave gauges were installed in the wave flume, three of which were located on the front wall of the OWC model, and the remaining mounted along the wave flume as shown in Figure 3. Three ultra-sonic wave sensors (shown in Figure 2) were installed inside the chamber of the OWC model (in the middle, left and right hand sides of the model) as well as one air pressure gauge sensor. The sampling frequency of all sensors was 20 *Hz*. The WG1 sensor was installed to detect the incident wave pattern at the beginning of each test before the reflected waves approach this sensor. The data gathered from the wave gauges WG3, WG4 and WG5 were used to analyse the incident and reflected wave characteristics during each experiment and the data measured from WG2 were considered as an alternative option for cases when disturbance or any interruption is occurred in those wave gauges. The data measured from the wave gauges WG6, WG7 and WG8 were used to be compared with the measurements of the ultra-sonic sensors.

Eventually, the data measured from the three ultra-sonic sensors and pressure gauges were used to evaluate the energy absorbed from the incoming waves. In this regard, the free surface

elevation ζ measured by the ultra-sonic sensor located in the middle of the OWC model (US2) and wave gauge WG1 as well as air pressure measured by the pressure gauge sensor (PS) are illustrated in Figure 4 for the regular waves with the period and height equal to 1.8 *s* and 0.04 *m,* respectively. As can be seen in Figure 4, the wave amplitude increases gradually between the time instants $t = 10$ and 15 seconds and remains constant after $t = 15\ s$, which is due to the approach of the reflected waves to the sensor (WG1) along with the incident waves generated by the paddle. It is also evident from Figure 4 that the amplitude of the free surface oscillations inside the OWC model as well as the amplitude of the pressure become stable and tend to have a constant value after the time instant around $t = 8\ s$, which proves the appropriate action of the AWACS system to absorb the reflected waves in the wave flume.

The OWC device was tested in both regular and irregular wave conditions. Two different damping conditions (high and low damping) were applied to the model by changing the slot width on the cap of the model. The slot width for the high and low damping conditions was adjusted as to be 1 and 2.5 mm, respectively. The water depth was set to 0.42 m and was kept constant during all the experiments. For the regular wave tests, ten wave periods ($T = 1, 1.2, 1.4, 1.6, 1.8, 2.0, 2.2, 2.4, 2.6$ and $2.8\ s$) and three wave heights ($H = 0.02, 0.04$ and $0.06\ m$) were combined. The duration of each test was designed in such a way that at least 100 individual waves were generated. In the irregular wave tests, four peak wave period ($T_p = 1.54, 1.98, 2.42$ and $2.86\ s$) with significant wave height of $H_s = 0.04\ m$ were applied. In addition, in the case of high damping condition, the model was tested in irregular waves with the significant wave height of $H_s = 0.08\ m$, too. Hence, 72 tests (60 tests in regular and 12 tests in irregular wave condition) were, in total, carried out to evaluate the performance of the device. The duration of each irregular wave test was defined so that at least 500 waves were generated. The irregular wave condition was generated in the flume based on the JONSWAP spectrum, which can be expressed as:

$$S(\omega) = g^2\omega^{-5}\exp\left\{-1.25\left(\frac{\omega}{\omega_p}\right)^{-4}\right\}\Gamma^{\exp\left(-\frac{(\omega-\omega_p)^2}{2(\sigma\omega_p)^2}\right)} \tag{35}$$

where ω_p is the peak angular frequency ($\omega_p = 2\pi/T_p$), Γ is the peak-enhancement factor and was set to 3.3, and σ is the shape parameter and is defined as:

$$\sigma = \begin{cases} \sigma_a = 0.07, & \omega \leq \omega_p \\ \sigma_b = 0.09, & \omega > \omega_p \end{cases} \quad (36)$$

3.3. Data analysis

The performance of the OWC device can be evaluated by estimating the incident wave power and the power absorbed from waves. The average power absorbed form regular waves $W_{Reg.}$ or random waves $W_{Ran.}$ can be determined using experimental data as follows:

$$W_{Reg.}\ or\ W_{Ran.} = \frac{1}{t_{max}} \int_0^{t_{max}} P\ Q\ dt \quad (37)$$

where t_{max} is the duration of the test, P is the air pressure inside the OWC chamber measured by the pressure gauge sensor and Q is the air volume flux through the slot of the OWC model. The air flow can be assumed as an incompressible flow due to the small volume of air trapped inside of the model. Hence, the air volume flux Q can be estimated implementing the water free surface elevation ζ_i inside of the OWC detected by the three ultra-sonic sensors installed inside the model as follows:

$$Q = LbD^3(\zeta_i) \quad (38)$$

where L is the width of the chamber perpendicular to the incident wave direction, b is the length of the chamber (parallel to the incident wave direction) and $D^3(\zeta_i)$ is the third-order approximation to the time derivative of the free surface elevation which can be expressed as follows:

$$D^3(\zeta_i) = \frac{-11\zeta_i + 18\zeta_{i+1} - 9\zeta_{i+2} + 2\zeta_{i+3}}{6\Delta t} \quad (39)$$

where $\Delta t = 0.05\ s$ is the time step between two consecutive data points.

It should be noted that the free surface elevation ζ_i inside the OWC chamber at time t_i, is calculated by means of averaging the data gathered from the three ultra-sonic sensors at each time instant.

In order to determine the incident wave power for both regular and random waves, the data measured by the wave gauges WG3, WG4 and WG5 are used to estimate the energy spectrum of the incoming waves. As part of the incoming waves is always reflected upon intercepting

the model, the data measured by the wave gauges are the combination of both incoming and reflected waves. In this regard, the method of Mansard and Funke (1980) is used to decompose incoming and reflected wave data from each other and on that basis the energy spectrum of the incoming waves is determined. It is noteworthy to remark that Viviano et al. (2016) reported that the accuracy level of this method is satisfactorily enough to estimate the incident and reflected wave pattern and hence could be reliably used here in the analysis procedure. In this context, figure 5 illustrates an example of incident and reflected water elevation spectra achieved by applying the method of Mansard and Funke (1980) for the case of regular wave with $T = 1.2\ s$ and $H = 0.02\ m$. Both spectra are perfectly narrow banded (which correspond to the single frequency of the regular wave) and their spiked peaks occur at $\omega = 5.24\frac{Rad}{s}$ which is consistent perfectly with the applied wave period $T = 1.2\ s$ to the wave maker device. The ratio of the reflected wave energy to the incident wave energy is one of the possible alternatives to estimate the performance of the device which is avoided to use here as some part of the energy is always lost due to occurring viscous phenomena. Hence, only the incident wave spectra as well as the data recorded from ultra-sonic sensors and air pressure gauge are used to estimate the captured and incident wave power. In this regard, by substituting the associated incoming wave spectrum S into Eqn. (32), the average incident wave power can be calculated for both regular and random wave conditions. By determining both incident wave power and absorbed power by the OWC device, the efficiency of the device can be estimated using Eqns. (21) and (31) for regular and random waves, respectively.

4. Results and discussion

In this section, the results obtained from numerical modelling and experimental studies of the OWC model with characteristics shown in the Figure 2 are presented. In both numerical and experimental approaches, the focus is mostly on the evaluation of the performance of the OWC in regular and random waves. Furthermore, the validity of the numerical approach was evaluated by comparing the corresponding results with the results achieved from the experimental study.

In spite of the typical fixed and floating structures which are strived in their design procedure to prevent the occurrence of any resonance phenomenon, the resonance mechanism arisen from the hydrodynamic interaction of the incident waves with the water column inside the OWC device can improve the efficiency of the device. In principle, two different possible

448 resonance phenomena can occur in the conventional fixed type OWC devices. The first
449 resonance mechanism, which is the dominant one, occurs due to the adaption of the frequency
450 of the incoming waves and the natural frequency of the water column inside the chamber of
451 the OWC. By the occurrence of this resonance phenomenon, the performance of the OWC
452 device tends to be maximized.

453 In this regard, the associated angular frequency can be estimated to be approximately equal to:

454 $$\omega = \sqrt{\frac{g}{a}} \tag{40}$$

455 where a is the length of immersion of the OWC device and g is the acceleration due to
456 gravity. The above mentioned formula is developed using the simple hydrostatic balance
457 equations by considering the water inside the OWC as a rigid piston. It gives satisfactory
458 predictions when the water column inside the enclosed volume of the OWC is narrow and
459 hence has a reciprocating motion similar to a piston due to the action of the incoming waves
460 (Evans and Porter, 1995 and Rezanejad et al., 2013). In the OWC model studied in this paper
461 (shown in Figure 2), the approximate angular frequency of the first resonance phenomenon is
462 predicted to be equal to $\omega \cong 12.8\ Rad/s$ ($T \cong 0.5\ s$) implementing Eqn. (40). The added mass
463 of the water column inside the OWC chamber is neglected in simplified formulation
464 introduced in the Eqn. (40) which may cause significant discrepancies to occur amongst
465 obtained predictions and realistic conditions. In this regard, van't Veer and Tholen (2008)
466 introduced an approximate expression to estimate the angular frequency of the first resonance
467 condition by considering the influence of the added mass as follows:

468 $$\omega = \sqrt{\frac{g}{a + 0.41\sqrt{S}}} \tag{41}$$

469 where S is the sectional area of the OWC chamber. Hence, the resonant angular frequency of
470 the studied OWC is predicted by Eqn. (41) to be equal to $\omega \cong 7.5\ Rad/s$ ($T \cong 0.84\ s$).

471 The second resonance mechanism occurs when the incident wave frequency is such that the
472 fluid inside the chamber is excited into an anti-symmetric sloshing mode. The appropriate
473 condition for the occurrence of this phenomenon can approximately be associated with cases
474 when $kb = n\pi$, where n is the sloshing mode number. It should be noted that the accuracy
475 level of the above mentioned formula is improved by increasing the submergence length of
476 the OWC. Therefore, the first mode of the sloshing resonance phenomenon occurs

approximately in the incident wave length of $25.6\ cm$ (equivalent to $T \cong 0.4\ s$) for the case of the OWC model investigated in this paper. The wave length for the occurrence of the higher modes of the sloshing phenomenon is even shorter than the first mode and does not lie in the generation range of the paddle. Hence, the second resonance mechanism which is dedicated to the sloshing phenomenon is not expected to occur in the OWC model considered in this study.

4.1. Comparison between experimental and numerical results

The primary efficiency of the OWC device is one of the most prominent issues that should be considered in the design procedure of the OWC devices. The primary efficiency, which is termed here as the efficiency or performance of the OWC device, indicates the percentage of the incident wave energy converted to pneumatic energy. In this section, the performance of the OWC model shown in Figure 2 was estimated using numerical and experimental methods following the approaches introduced in Sections 2 and 3. In this regard, Figure 6 illustrates the efficiency of the OWC model $\eta_{Reg.}$ in regular waves with respect to the incident wave period, which was obtained from the numerical simulation and the experimental tests for low and high damping conditions. The wave height was equal to $H = 2\ cm$ in the associated experimental tests and slot width was equal to $e = 1$ and $2.5\ mm$ for the high and low damping conditions, respectively. It is noteworthy to remark that the calculated performance is not dependent on the wave height in the numerical approach as the linear wave theory was implemented in formulating the problem. The least squares method was implemented in the numerical approach to determine the appropriate linear turbine damping coefficient λ in such a way that the calculated performance had the best fit to the corresponding experimental data. In order to find the damping coefficient λ associated with the damping of the PTO system, the efficiency of the OWC is assessed in regular waves (using Eqn. 23) for a range of damping values varying between 10^{-5} to $10^{-3}\ m^4.s/kg$ with the evenly distributed increments equal to $10^{-7}\ m^4.s/kg$. The discrepancies occurred between obtained numerical and experimental results for the each set of damping values are calculated and the least squares method was applied to assess the goodness of the each fit. Eventually, the damping coefficient dedicated to the best fitted line is considered as a damping of the system for the each low and high damping case. Following this approach, the linear damping coefficients were estimated to be equal to $1.208 \times 10^{-4}\ and\ 5.072 \times 10^{-4}\ m^4.s/kg$ for high and low damping conditions, respectively, and were kept as a fixed parameter in the rest of the numerical calculations. On the other hand, the damping coefficient corresponds in principle to the assumed linear

relationship between the air volume flux (q) and pressure (p) (Eqn. 16). As was explained earlier, the damping coefficient λ is estimated here using the indirect method based on approaching the best fit between the numerically and experimentally calculated efficiency curves. However, the estimated damping coefficients are also expected to be consistent with the general trend of air flux and air pressure variations in each instant. In this regard, Figure 7 shows the variation of the air flux and pressure inside the OWC chamber obtained from the regular wave test with the $T = 1.2\,s$ and $H = 0.02\,m$ for the high and low damping conditions. Although the pressure drop is in principle proportional to the square of the flow rate passing through the orifice, however, as can be seen here in the figure 7, the damping lines (plotted based on the estimated damping coefficients) are also in a satisfactory agreement with the experimental data. It should be also remarked that to plot the damping lines, the estimated linear damping coefficients $1.208 \times 10^{-4}\ and\ 5.072 \times 10^{-4}\ m^4.s/kg$ are multiplied to the OWC width, $L = 0.61\,m$, as they were estimated based on the 2D calculations (the width of the device perpendicular to the wave direction is assumed to have the unit value).

As can be seen in Figure 6, the agreement between numerical and experimental predictions for both damping conditions is satisfactory. Furthermore, the maximum theoretical efficiency $\eta_{Reg.,max}$ determined from Eqn. (25) is shown in this figure. The maximum efficiency takes the unity value at the period of $T = 0.75\,s$ which corresponds to the first resonance mechanism. As explained in the previous section, the simplified formula of Eqn. (40) predicts the value of $0.5\,s$ for the period of the maximum efficiency, which has a difference to the value obtained from the numerical simulations. The difference between predictions obtained from these two methods is mainly due to ignoring the share of the added mass in this formulation. On the other hand, the formula introduced in Eqn. (41) gives more precise prediction regarding the resonance period of OWC (which is $T = 0.84\,s$ as explained earlier in the section 4) as the role of the added mass is included in the proposed formulation.

As can be expected, the OWC model has higher performance in high damping condition than in low damping case and the maximum efficiency is not unity for both damping conditions. The maximum efficiency of both high and low damping conditions occurs almost in the same period of the peak of the maximum efficiency curve, which proves that the period for which the first resonance mechanism takes place is not dependent on the damping condition, and is mostly determined by the natural frequency of the water column. As was predicted in the

previous section, none of the efficiency curves contain the secondary peak due to the occurrence of the sloshing phenomenon. The maximum efficiency curve $\eta_{Reg.,max}$ shown in Figure 6 in principle represents the threshold of the power absorption capacity of the current geometrical configuration of the system. Hence, it can be concluded that the performance of the system in the case of high damping condition is satisfactory in the small and medium wave periods as the corresponding efficiency has almost slight decrease with respect to the maximum efficiency curve. On the other hand, the efficiency of the system decreases significantly with respect to the maximum efficiency in large wave periods. Furthermore, the efficiency curve has an undesirable drop almost in the whole range of wave periods in the low damping condition which leads to the essential decrease in the power production of the system rather than the optimized condition.

Figure 8 illustrates the efficiency of the OWC model in random waves $\eta_{Ran.}$ with respect to the peak wave period for both low and high damping conditions. The random waves are generated using the JONSWAP spectrum in both numerical and experimental approaches. Also, the optimized efficiency of the OWC model in random waves obtained from the numerical simulation is introduced in this figure. In order to estimate the optimized efficiency, the damping of the OWC model is considered to have a fixed value in each sea state which is determined by Eqn. (24) for the equivalent regular wave with the period equal to the T_e (energy period in random waves). It should be noted that basically there is no analytical method devised yet for estimating the optimized damping coefficient in irregular waves (Bull, 2015 and Sheng and Lewis, 2016) as random waves are composed of individual wave components with various frequencies. However, the efficiency calculated based of the above mentioned approach will be called here as "optimized efficiency" since the damping of the system in each sea state is chosen to have the constant value equal to the optimum damping value of the equivalent regular wave. The two low and high damping coefficients determined in the regular wave analysis procedure are considered to remain unchanged in the random wave analysis. As is evident in Figure 8, both numerical and experimental approaches produce consistent results. The efficiency curve in random waves follows in general the same trend of variations as in the regular waves. However, it is slightly smoother in random waves which can be related to the nature of the irregular waves that contain various individual waves. Similarly to the regular wave condition, the efficiency of the OWC model in random waves is higher for the high damping condition and is almost close to the optimized efficiency curve. It should be noted that the optimized efficiency curve is probably not the maximum

efficiency that could be captured from the random waves and it would be possible to improve the performance of the system by the application of an appropriate active control procedure for the turbine damping characteristics.

4.2. OWC primary efficiency: effect of the damping and incident wave period

The numerically estimated performance of the OWC model in regular wave conditions versus the wave period and turbine damping coefficient are illustrated in Figure 9. As can be detected from this figure, both wave period and turbine damping coefficient have the dominant influence on the performance of the device and hence should be considered as most prominent parameters to design an OWC device for a specific wave climate. It can also be observed that the occurrence period of the maximum efficiency in each specific turbine damping occurs approximately for the same wave period ($T = 0.75\ s$) as reported in the previous section too.

As is evident in Figure 9, the absolute maximum efficiency of the OWC model is less sensitive to the small variations in the turbine damping coefficient. Therefore, the damping coefficient can be chosen in the range of 1.5×10^{-4} to $5 \times 10^{-4}\ m^4.s/kg$ in order to capture over 90 percent of the incoming wave energy with the period around $0.75\ s$ which is an appropriate point in the design procedure of the turbine control system. The efficiency of the device significantly drops for large wave periods and just for the small ranges of the turbine damping coefficient (between 1.2×10^{-5} to $3.6 \times 10^{-5}\ m^4.s/kg$) it approaches the value around 20 percent. As the waves with large periods contain large amount of energy, it is essential to set up the turbine in such a way that imposes appropriate damping to the system to absorb the energy of waves. Otherwise the waves would be reflected back to the sea upon encountering the device without their energy being captured.

It should be noted that the abrupt drop of the efficiency outside of the above mentioned range of the damping coefficient is due to the small magnitude of the conductance parameter $\hat{B}$ in large wave periods (Rezanejad et al., 2013) which causes the numerator of the efficiency expression in Eqn. (23) to tend to have a zero value while the denominator could remain as a non-zero value due to the influence of the turbine damping coefficient λ. Hence, the efficiency of the device tends to have a small value in the large wave periods and in the extensive ranges of turbine damping coefficient.

The curve showing the respective values of the optimum turbine damping on which the maximum efficiency occurs in each wave period is also shown in Figure 9 by the solid black line. It can be seen from Figure 9 that the variation of the optimum turbine damping is small for the wave periods larger than two seconds and could be considered as a fixed value (approximately equal to $3.6 \times 10^{-5}\, m^4.s/kg$) and hence the control tool installed in the device should only impose this amount of damping to the system to maximize energy absorption of the device. On the other hand, there is significant variation in the optimum turbine damping for waves with periods less than two seconds (in the range of 0.5×10^{-4} to $3 \times 10^{-4}\, m^4.s/kg$) and hence the control system should alter the damping of the turbine under the action of the changings occurring in the incident wave period.

4.3. OWC primary efficiency: effect of the incident wave height

In order to discern the influence of the wave height on the performance of the OWC device, three different wave heights ($H = 0.02, 0.04$ and $0.06\, m$) in regular waves as well as two significant wave heights ($H_s = 0.04$ and $0.08\, m$) are applied in the experimental campaign. Figure 10 illustrates the variations of the OWC efficiency with respect to the wave period for the three individual wave heights in the regular wave condition as well as the results achieved from numerical approach. The results shown in Figure 10 only correspond to the high damping condition, whereas the respective results of the low damping case are introduced in Figure 11. It is evident in these figures that the relation of the wave height to the efficiency of the device is more complex. As can be seen in Figure 10, higher wave height results in higher efficiency of the device in large wave periods ($T \geq 1.6s$) and on the contrary, results in lower performance for small periods of the incoming waves ($T \leq 1.2s$) in high damping condition. In other words, as wave height increases, the efficiency curve of the device tends to have a smoother variation with respect to the wave period.

Hence, the numerical results obtained from linear modelling of the device should be used cautiously for large wave heights as a significant deviation between numerical predictions and real condition could arise. On the other hand, increasing the wave height enhances the performance of the OWC device in the low damping condition regardless of the variations in wave period as can be seen in Figure 11. In order to better understand the impact of the wave height by simultaneously considering the variations of the wave period, the efficiency of the OWC model is presented in Figure 12 for both high and low damping conditions in regular

635 waves. In general, it can be concluded that the influence of the wave height is of lesser
636 significance on the efficiency of the OWC model than on the wave period, although it would
637 become a prominent parameter as the damping of the system increases.

638 A similar behaviour is also detected for the random waves, as can be observed in Figure 13.
639 This figure corresponds to the high turbine damping condition. Similarly to the regular wave
640 condition, higher significant wave height results in higher efficiency in larger periods and
641 lower efficiency in smaller ones, although the rate of variation is not as significant as in
642 regular waves which is due to the occurrence of various wave periods in each sea state.

643 ## 5. Conclusions

644 The performance of the Oscillating Water Column (OWC) device was studied in this paper
645 based on both numerical and experimental approaches. A 2D linear model is developed in the
646 numerical approach and the results achieved from the frequency domain analysis are used to
647 estimate the efficiency of the device in both regular and random wave conditions. A
648 comprehensive set of experiments is carried out in regular and random wave conditions in
649 order to evaluate the accuracy level of the numerical method as well as to investigate the
650 influence of the turbine damping, wave height and period.

651 It is observed in both numerical and experimental results that the wave period and turbine
652 damping have a dominant influence on the performance of the device and hence ought to be
653 in the focus of attention in the optimizing procedure of the OWC device. The performance of
654 the device drops significantly in high wave periods and becomes very sensitive to the
655 variation of the turbine damping. The absolute maximum efficiency of the device mainly
656 depends on the wave period and becomes less sensitive to the minor variations imposed to the
657 optimum value of the turbine damping. The influence of the wave height on the performance
658 of the OWC device is of lesser importance as compared to the two other parameters (wave
659 period and turbine damping) and causes the efficiency curve become smoother with respect to
660 the variations of wave period.

661 **Acknowledgements**

662 The work has been conducted within the Strategic Research Plan of the Centre for Marine
663 Technology and Ocean Engineering, which is financed by Portuguese Foundation for Science
664 and Technology. The first author has been funded by the Portuguese Foundation for Science

and Technology (Fundação para a Ciência e Tecnologia – FCT) under contract SFRH/BD/98287/2013. The experimental part of the work was conducted in the wave flume of the Hydraulics Laboratory integrated in the Group of Civil Engineering and Marine Energies (GICEMA), Escuela Politécnica Superior based on the scientific cooperation agreement between Instituto Superior Técnico and University of Santiago de Compostela.

References

Anvesh, V., Karmakar, D., Guedes Soares, C., 2016. Performance of oscillating water column wave energy converters integrated in breakwaters. Guedes Soares, C., (Ed.). Progress in Renewable Energies Offshore. London, UK: Taylor & Francis Group, 295-302.

Ashlin, S. J., Sundar, V., Sannasiraj, S. A., 2016. Effects of bottom profile of an oscillating water column device on its hydrodynamic characteristics. Renewable Energy 96, 341-353.

Bahaj, A. S., 2011. Generating electricity from the oceans. Renewable and Sustainable Energy Reviews 15: 7, 3399–3416.

Bull, D., 2015. An improved understanding of the natural resonances of moonpools contained within floating rigid-bodies: Theory and application to oscillating water column devices. Ocean Engineering 108, 799-812.

Clément, A., McCullen, P., Falcão, A., Fiorentino, A., Gardner, F., Hammarlund, K., Lemonis, G., Lewis, T., Nielsen, K., Petroncini, S., Teresa Pontes, M., Schild, P., Sjöström, B. O., Sørensen, H. C., Thorpe, T., 2002. Wave energy in Europe: current status and perspectives. Renewable and Sustainable Energy Reviews 6: 5, 405–431.

Crema, I., Simonetti, I., Cappietti, L., Oumeraci, H., 2015. Laboratory Experiments on Oscillating Water Column Wave Energy Converters Integrated in a Very Large Floating Structure. Proceedings of the 11th European Wave and Tidal Energy Conference, 6-11th Sept., Nantes, France.

Cruz, J., 2008. Ocean wave energy: Current Status and Future Perspectives. Heidelberg: Springer.

Dean, R.G., Dalrymple, R.A., 2001. Water wave mechanics for Engineers and Scientists. New Delhi: Allied Publishers limited.

Evans, D.V., 1976. A theory for wave power absorption by oscillating bodies. Journal of Fluid Mechanics 77: 1, 1-25.

699 Evans, D.V., 1981. Power from water waves. Annual Review of Fluid Mechanics 13,
700 157-187.
701 Evans, D.V., 1982. Wave-power absorption by systems of oscillating surface pressure
702 distributions. Journal of Fluid Mechanics 114, 481-499.
703 Evans, D.V., Porter, R., 1995. Hydrodynamic characteristics of an oscillating water
704 column device. Applied Ocean Research 17, 155-164.
705 Falcão, A.F. de O., Rodrigues, R.J.A., 2002. Stochastic modelling of OWC wave
706 power plant performance. Applied Ocean Research 24: 59-71.
707 Falcão, A., 2010. Wave energy utilization: A review of the technologies. Renewable
708 and Sustainable Energy Reviews 14: 3, 899-918.
709 Falcão, A. F., Cândido, J. J., Justino, P. A., Henriques, J. C., 2012. Hydrodynamics of
710 the IPS buoy wave energy converter including the effect of non-uniform acceleration
711 tube cross section. Renewable energy 41, 105-114.
712 Falcão, A. F. O., Henriques, J. C. C., 2014. Model-prototype similarity of oscillating-
713 water-column wave energy converters. International Journal of Marine Energy 6, 18-
714 34.
715 Falnes, J., McIver, P., 1985. Surface wave interactions with systems of oscillating
716 bodies and pressure distributions. Applied Ocean Research 7: 4, 225-234.
717 Falnes, J., 2002. Ocean waves and oscillating systems: linear interactions including
718 wave-energy extraction. Cambridge university press.
719 Falnes, J., 2007. A review of wave-energy extraction. Marine Structures 20: 4, 185-
720 201.
721 Gervelas, R., Trarieux, F., Patel, M. A., 2011. A time-domain simulator for an
722 oscillating water column in irregular waves at model scale. Ocean Engineering 38: 8-
723 9, 1007-1013.
724 Guedes Soares, C., Bhattacharjee, J., Tello, M., and Pietra, L. 2012. Review and
725 classification of Wave Energy Converters. Guedes Soares, C., Garbatov, Y., Sutulo,
726 S., Santos, T. A., (Eds.). Maritime Engineering and Technology. London, UK: Taylor
727 & Francis Group, 585-594.
728 Ikoma, T., Osawa, H., Masuda, K., Maeda, H., 2011. Expected values of wave power
729 absorption around the Japanese islands using OWC types with projecting walls. Proc.
730 of the 30th International Conference on Ocean, Offshore and Arctic Engineering, June
731 19-24, Rotterdam, The Netherlands, Paper no. OMAE2011-49685, 573-580.

López, I., Pereiras, B., Castro, F., Iglesias, G., 2014a. Optimisation of turbine-induced damping for an OWC wave energy converter using a RANS–VOF numerical model. Applied Energy 127, 105–114.

López, I., Pereiras, B., Castro, F., Iglesias, G., 2014b. Performance of OWC wave energy converters: influence of turbine damping and tidal variability. International Journal of Energy Research 39: 4, 472-483.

López, I., Iglesias, G., 2014. Efficiency of OWC wave energy converters: A virtual laboratory. Applied Ocean Research 44, 63–70.

Mansard, E.P.D., Funke, E.R., 1980. The measurement of incident and reflected spectra using a least square method. Proceedings of the 17th International Conference on Coastal Engineering, Sydney, Australia, 154–172.

Mei, C.C., 1976. Power extraction from water waves. Journal of Ship Research 20, 63-66.

Ning, D.Z., Shi, J., Zou, Q.P., Teng, B., 2015. Investigation of hydrodynamic performance of an OWC (oscillating water column) wave energy device using a fully nonlinear HOBEM (higher-order boundary element method). Energy 83, 177–188.

Ning, D.Z., Wang, R. Q., Zou, Q.P., Teng, B., 2016. An experimental investigation of hydrodynamics of a fixed OWC wave energy converter. Applied Energy 168, 636–648.

Paris. F, Canas J., 1997. Boundary element method fundamentals and applications. Oxford University Press, ISBN 978 0 198 56543 7.

Rezanejad, K., Bhattacharjee, J., Guedes Soares, C., 2013. Stepped sea bottom effects on the efficiency of nearshore oscillating water column device. Ocean Engineering 70, 25–38.

Rezanejad, K., Bhattacharjee, J., Guedes Soares, C., 2015. Analytical and numerical study of dual-chamber oscillating water columns on stepped bottom. Renewable Energy 75, 272–282.

Rezanejad, K., Bhattacharjee, J., Guedes Soares, C., 2016. Analytical and numerical study of nearshore multiple oscillating water columns. Journal of Offshore Mechanics and Arctic Engineering 138, 021901 (7 pages).

Sheng, W., Alcorn, R., Lewis, A., 2014a. Assessment of primary energy conversions of oscillating water columns. I. Hydrodynamic analysis. Journal of Renewable and Sustainable Energy 6, p.053113.

765 Sheng, W., Alcorn, R., Lewis, A., 2014b. Assessment of primary energy conversions
766 of oscillating water columns. II. Power take-off and validations. Journal of Renewable
767 and Sustainable Energy 6, p.053114.
768 Sheng, W., Alcorn, R., Lewis, T., 2014c. Physical modelling of wave energy
769 converters. Ocean Engineering 84, 29-36.
770 Sheng, W., Lewis, A., 2016. Power Takeoff Optimization for Maximizing Energy
771 Conversion of Wave-Activated Bodies. IEEE Journal of Oceanic Engineering 41: 3,
772 529-540.
773 van't Veer, R., Tholen, H. J., 2008. Added resistance of moonpools in calm water.
774 Proceedings of the ASME 27th International Conference on Offshore Mechanics and
775 Arctic Engineering, June 15-20, Estoril, Portugal, Paper no. OMAE2008-57246, 153-
776 162.
777 Viviano, A., Naty, S., Foti, E., Bruce, T., Allsop, W., Vicinanza, D., 2016. Large-
778 scale experiments on the behaviour of a generalised Oscillating Water Column under
779 random waves. Renewable Energy 99, 875-887.
780

Table 1: Scale factor for various parameters based on the Froude criterion

Parameter	Unit	Scale factor for $\varepsilon = 25$
Wave amplitude, $\boldsymbol{A}$	m	$\varepsilon = 25$
Wave period, $\boldsymbol{T}$	s	$\varepsilon^{0.5} = 5$
Wave angular frequency, $\boldsymbol{\omega}$	Rad/s	$\varepsilon^{-0.5} = 0.2$
Pressure, $\boldsymbol{P}$	N/m^2	$\varepsilon = 25$
Volume flux, $\boldsymbol{q}$	m^3/s	$\varepsilon^{2.5} = 3125$
Power, $\boldsymbol{W_w}$	$N.m/s$	$\varepsilon^{3.5} = 78125$
Efficiency, $\boldsymbol{\eta}$	$-$	$\varepsilon = 1$

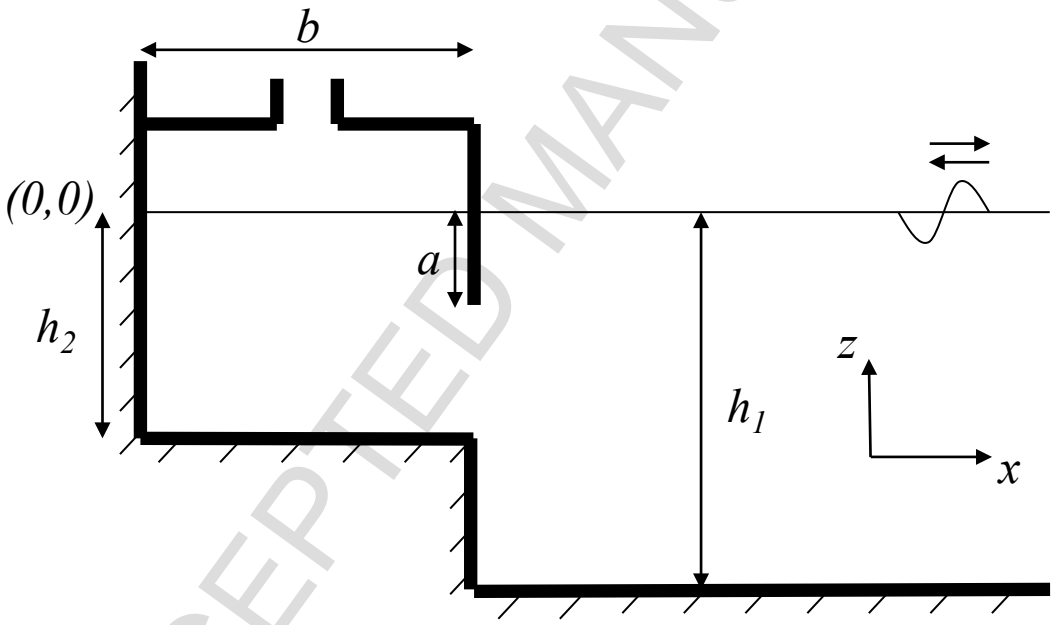

Figure 1: Sketch diagram for the numerical model of the OWC

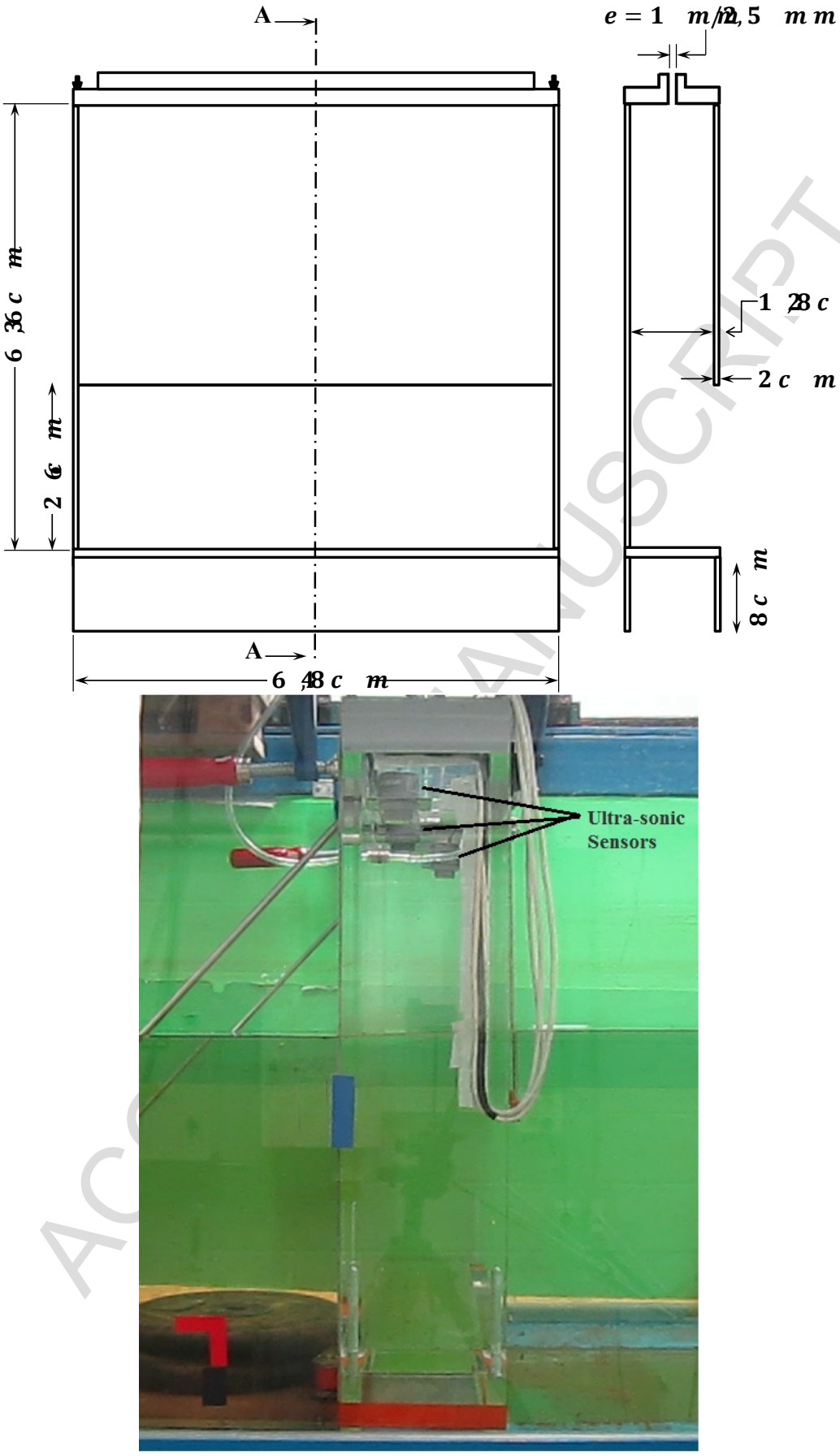

Figure 2: Physical model of the OWC device

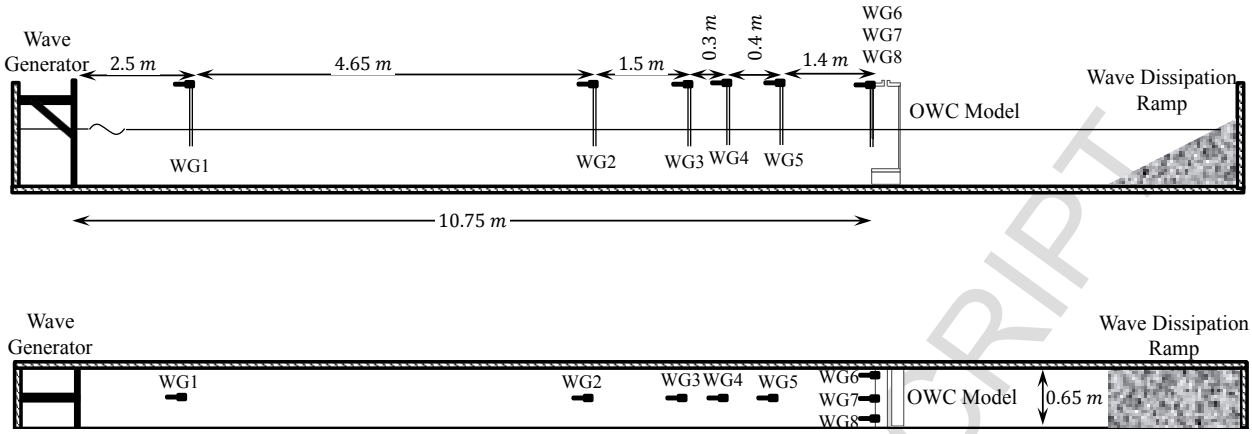

Figure 3: Sketch of the experimental setup

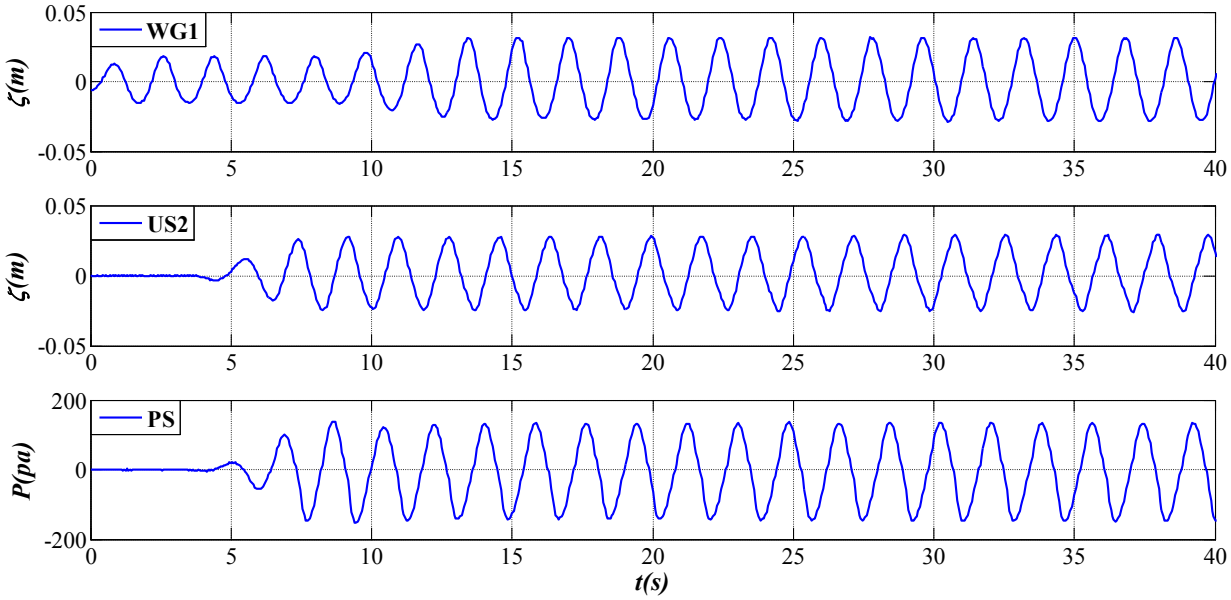

Figure 4: Data measured by the wave gauge WG1, ultra-sonic US2 and air pressure gauge sensors for the regular waves with the period and height equal to 1.8 s and 0.04 m

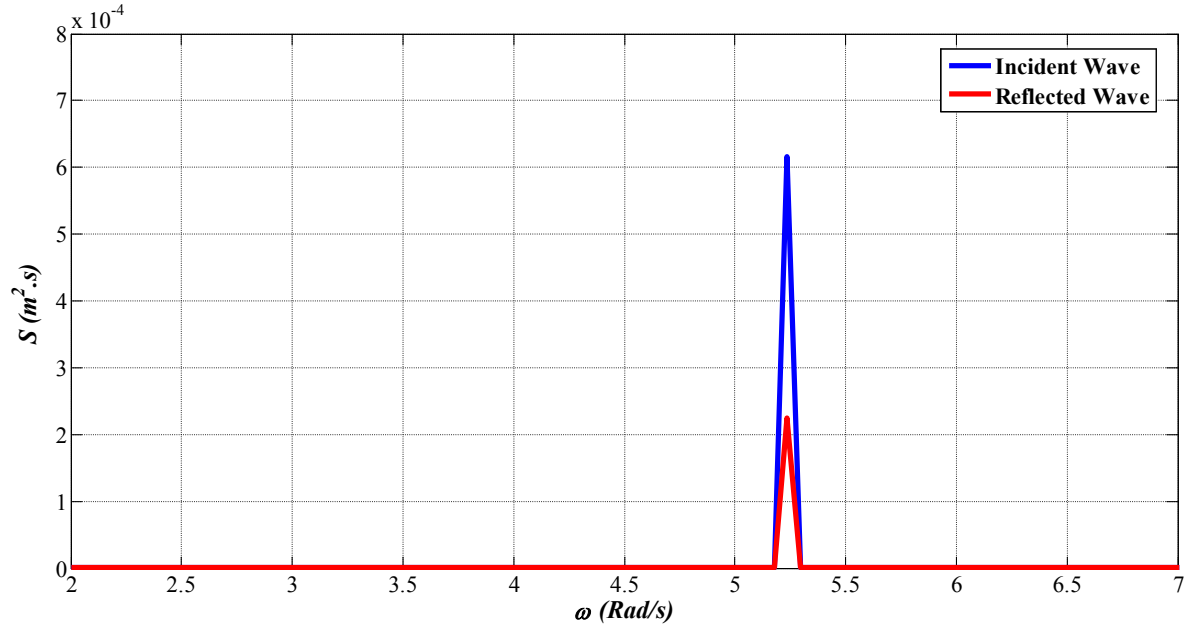

Figure 5: Incident and reflected spectra for the regular wave with $T = 1.2\ s$ and $H = 0.02\ m$ achieved by applying method of Mansard and Funke (1980) to the experimental data

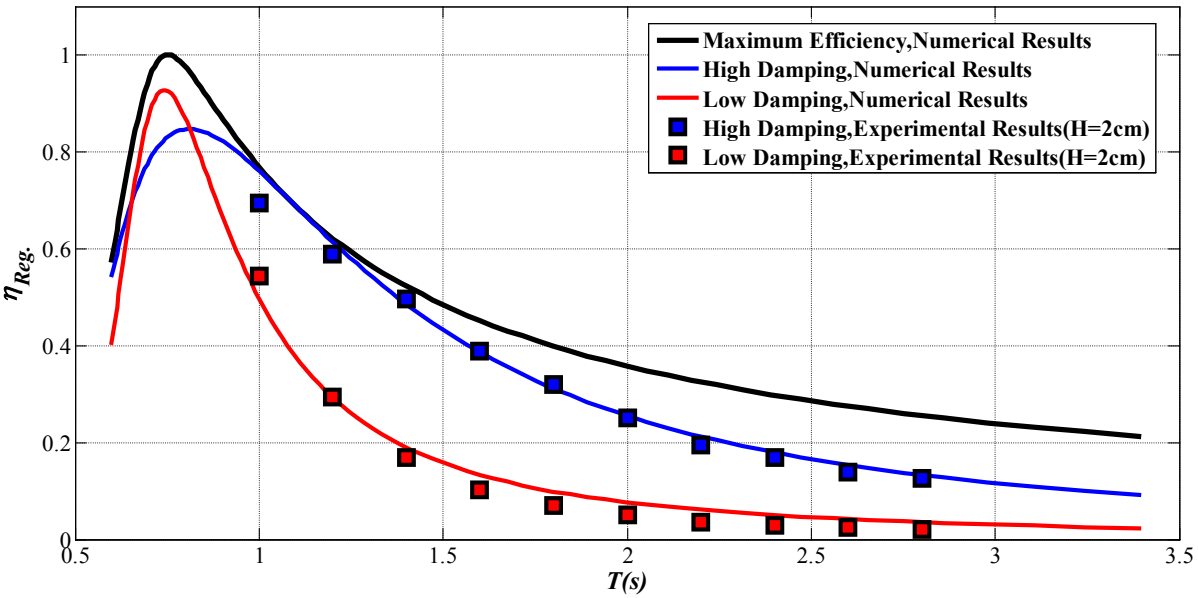

Figure 6: Efficiency of the OWC model in regular waves ($H = 2\ cm$) with respect to the wave period achieved from experimental tests and numerical simulation

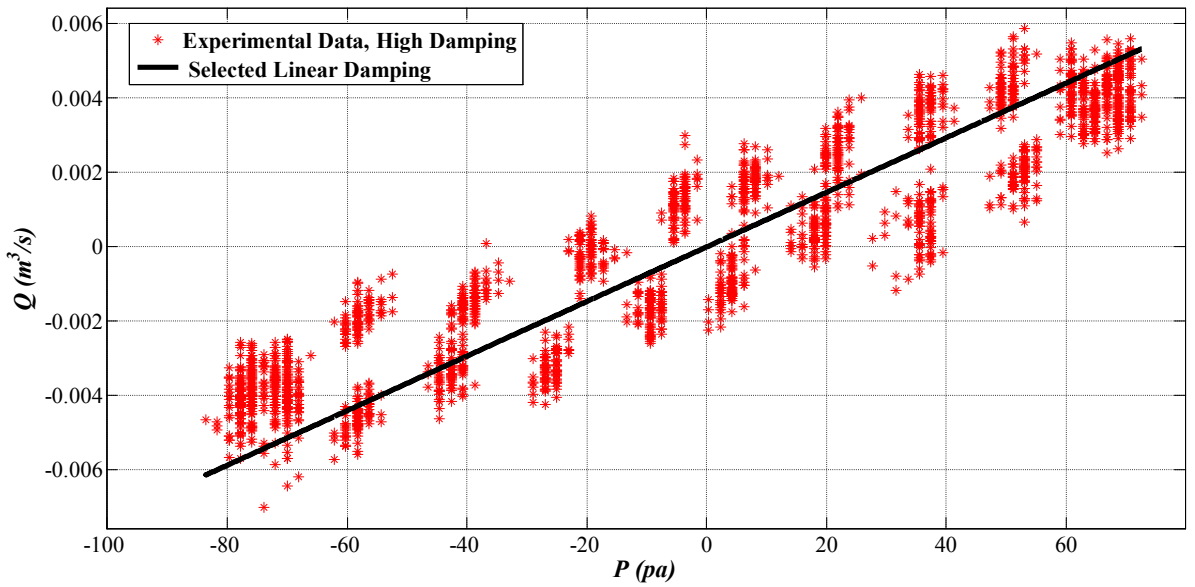

(a)

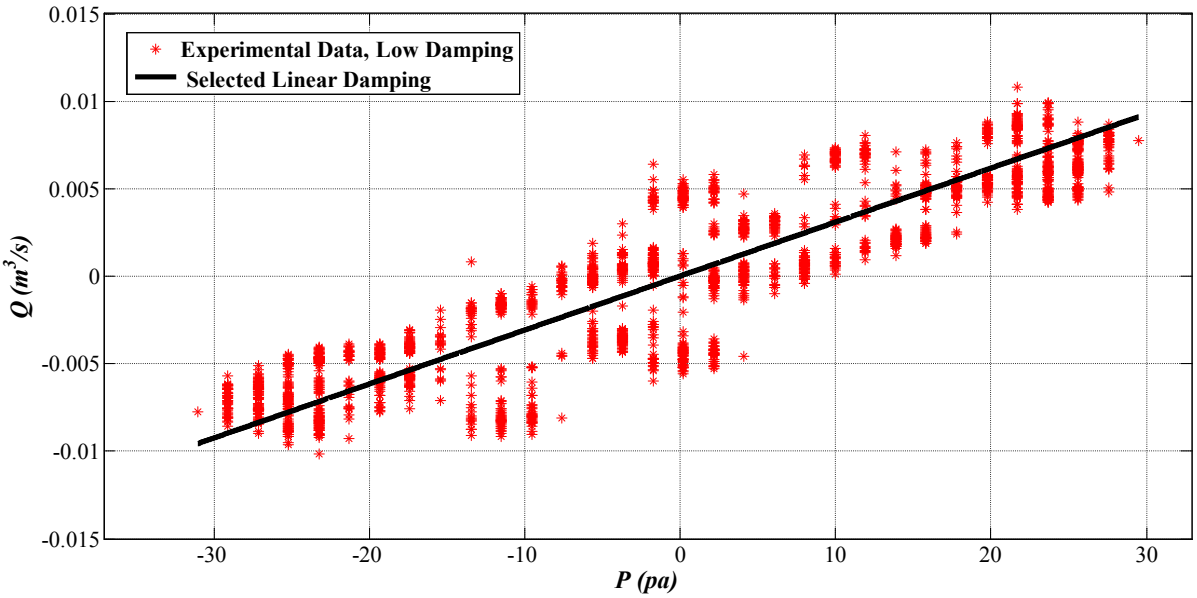

(b)

Figure 7: The air volume flux Q versus air pressure P achieved from the regular wave test with $H = 2\ cm$ and $T = 1.2\ s$ as well as the damping line (plotted based on the estimated linear damping coefficient) for the high (a) and low (b) damping cases

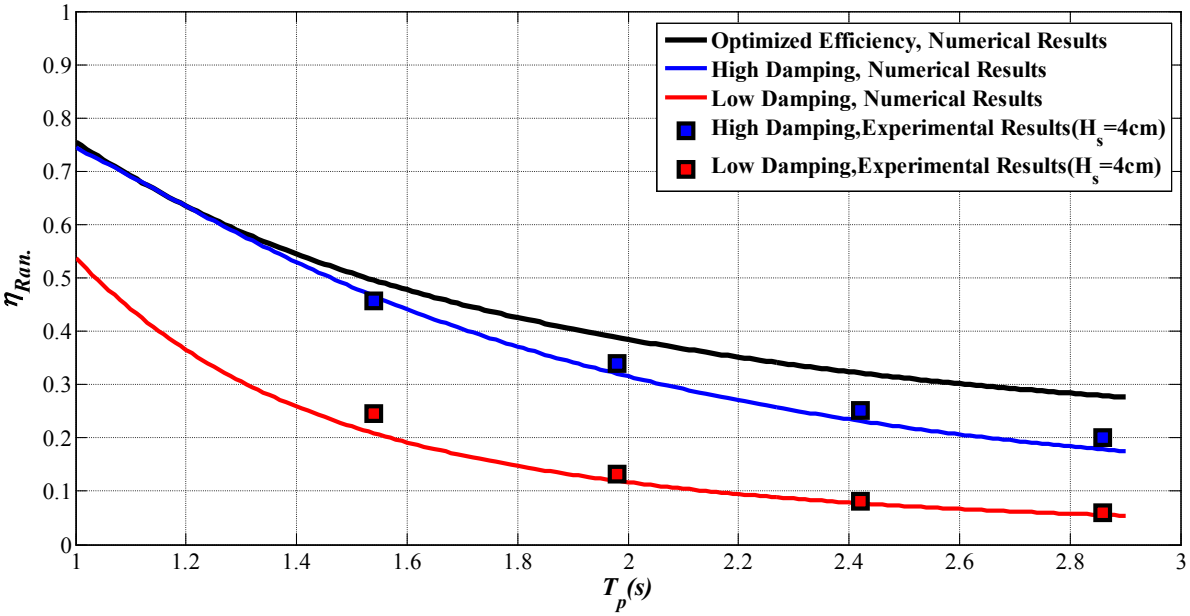

Figure 8: Efficiency of the OWC model in random waves (JONSWAP spectrum with $H_s = 4\ cm$) with respect to the peak wave period achieved from experimental tests and numerical simulation

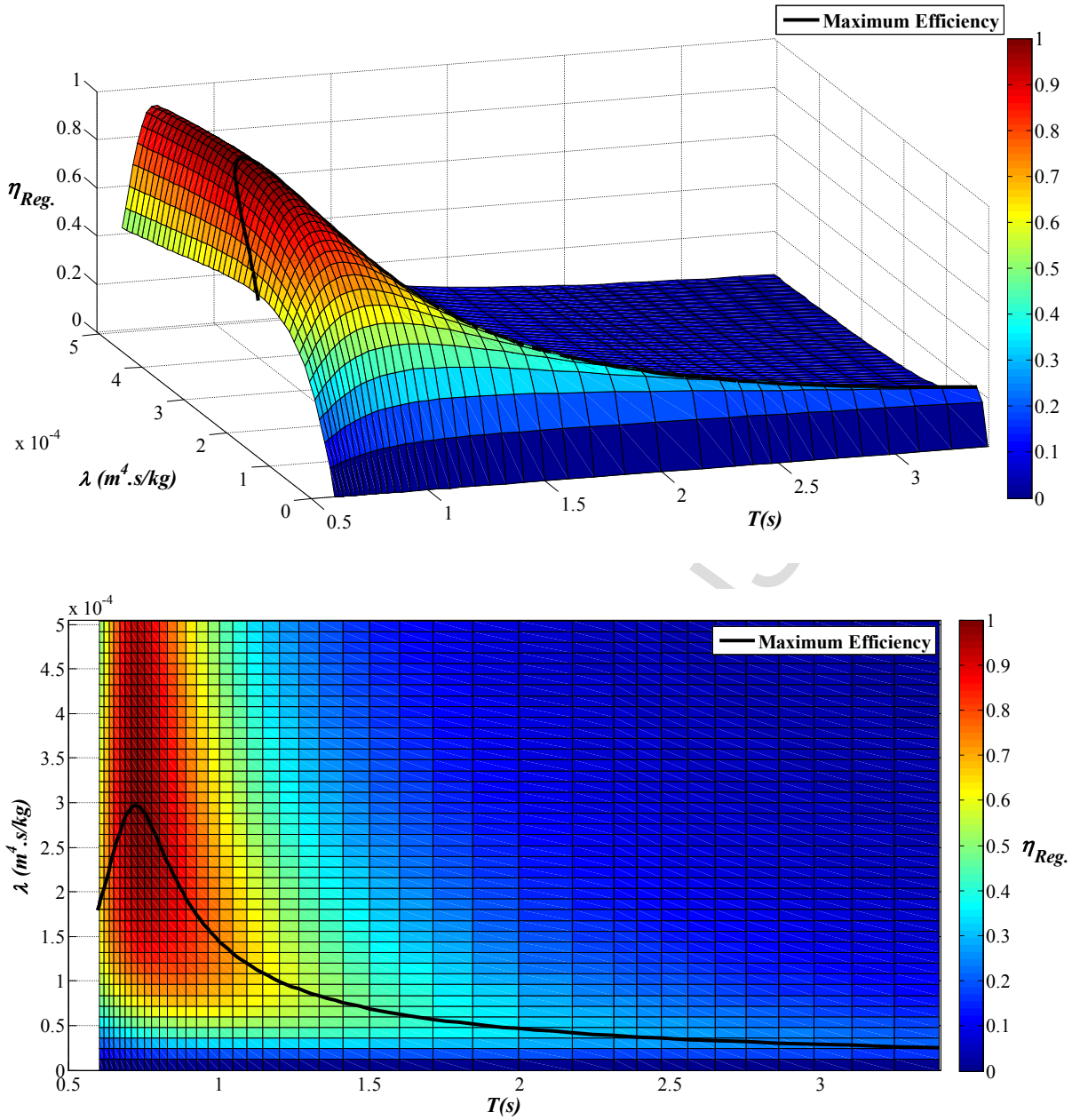

Figure 9: Efficiency of the OWC model in regular waves with respect to the wave period and turbine damping coefficient achieved from the numerical simulation

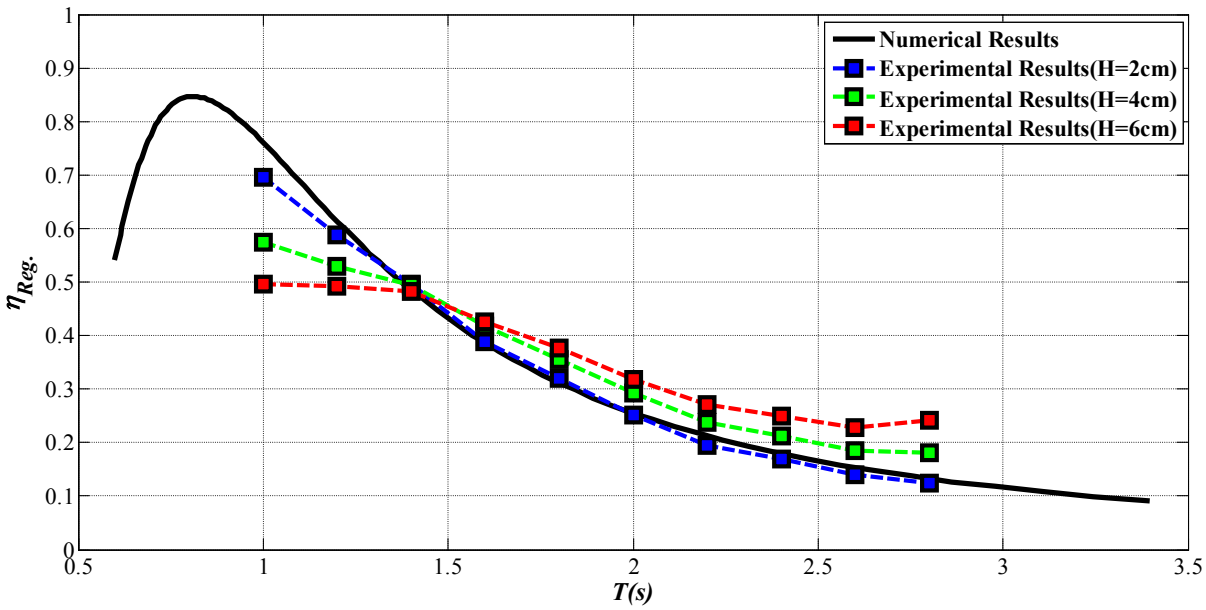

Figure 10: Efficiency of the OWC model in regular waves with respect to the wave period for the three individual wave heights as well as the results obtained from numerical simulation (high turbine damping condition)

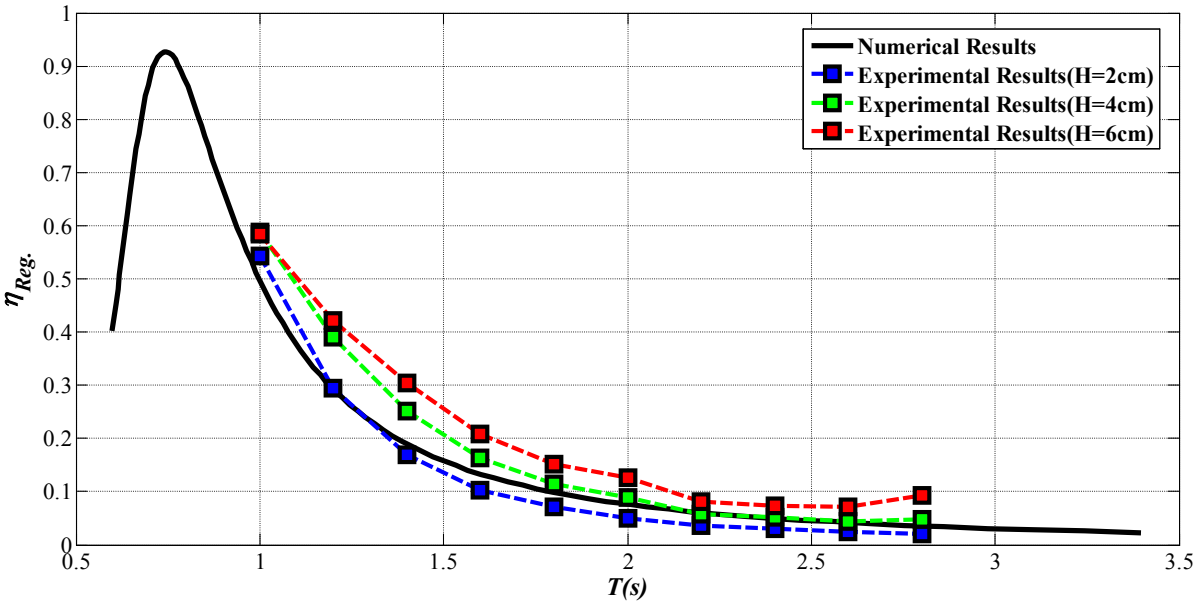

Figure 11: Efficiency of the OWC model in regular waves with respect to the wave period for the three individual wave heights as well as the results obtained from numerical simulation (low turbine damping condition)

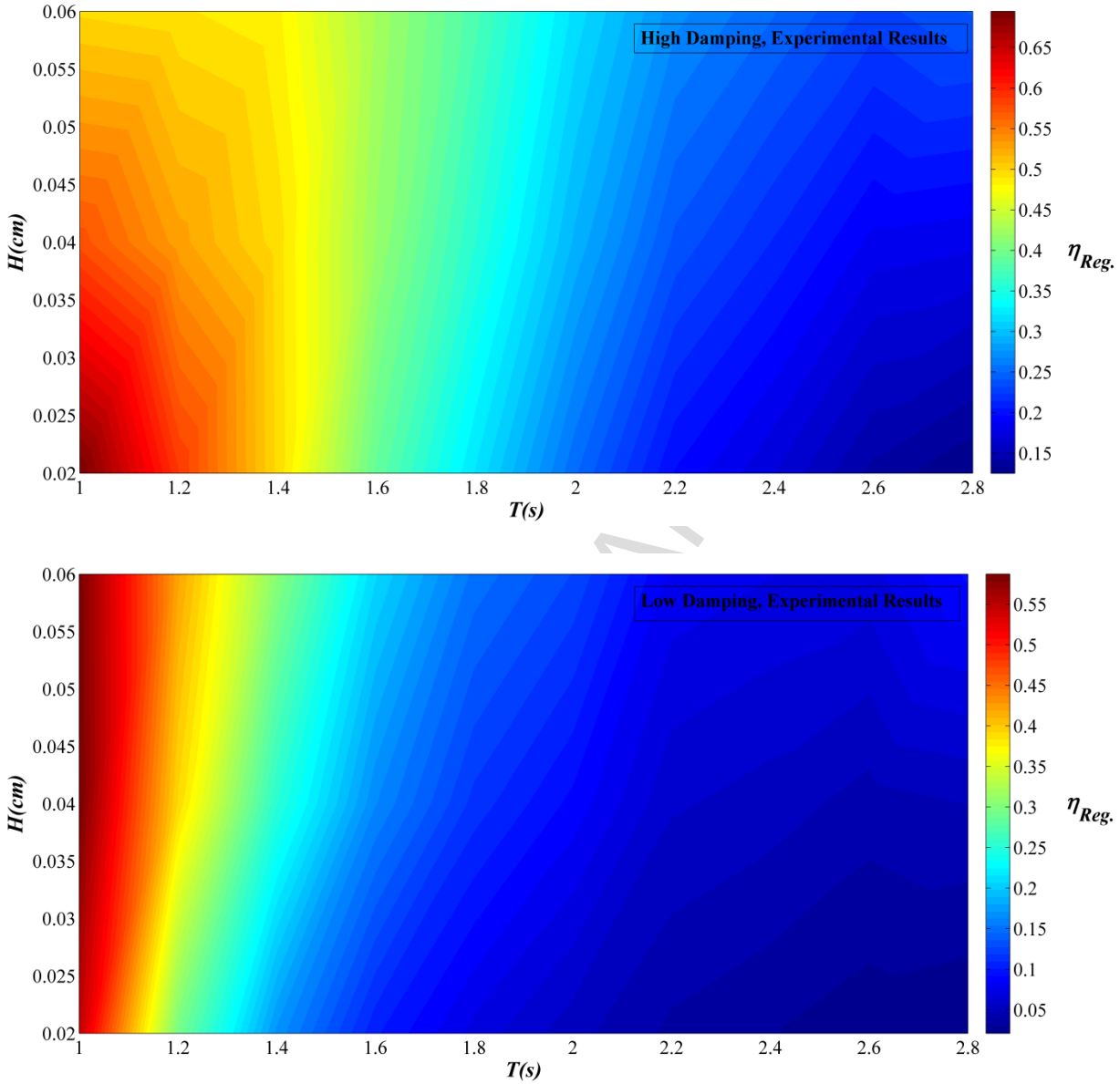

Figure 12: Efficiency of the OWC model in regular waves versus to the wave period and height for the high and low damping conditions

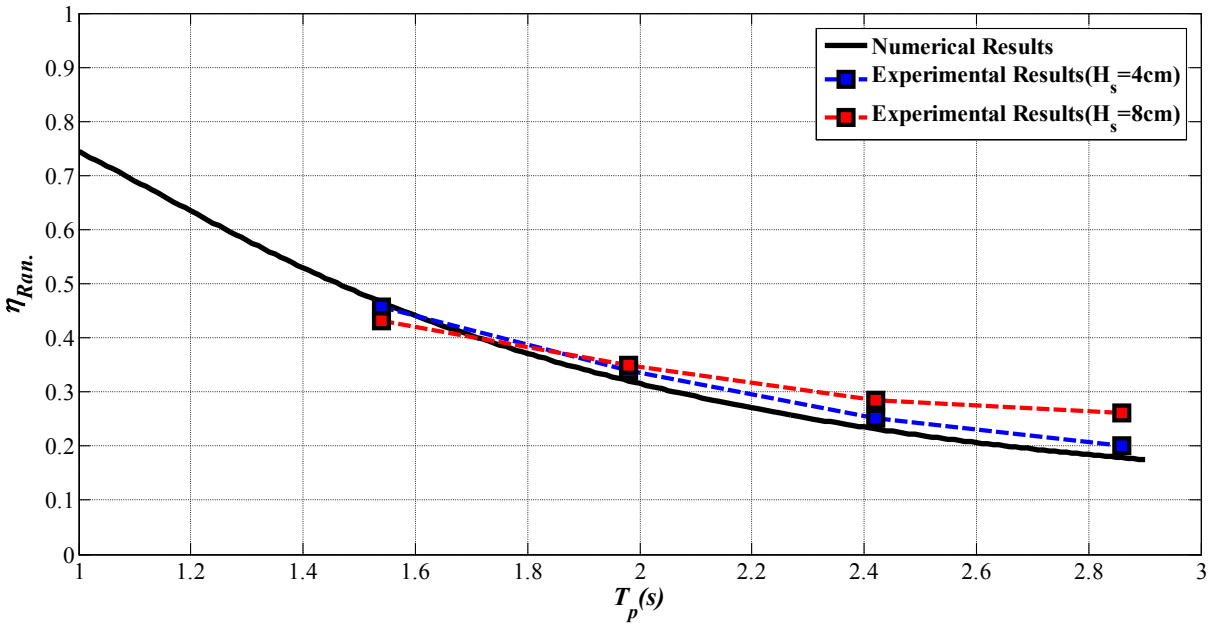

Figure 13: Efficiency of the OWC model in random waves with respect to the peak wave period for the two individual significant wave heights as well as the results obtained from numerical simulation (high turbine damping condition)